

國立交通大學
電子物理研究所
博士論文

Ⅲ-族氮化物表層缺陷研究

Investigation of interfacial defects
in Ⅲ-nitride

研究生：黃國欽

指導教授：黃凱風

中華民國 九十八年六月

III-族氮化物表層缺陷研究

Investigation of interfacial defects
in III-nitride

研究生：黃國欽 Student: Kuo-Chin Huang

指導教授：黃凱風 Advisor: Kai Feng Huang

國立交通大學

電子物理研究所

博士論文



A Dissertation

Submitted to Institute of Electrophysics
College of Science

National Chiao Tung University
in partial fulfillment of the Requirements
for the Degree of
Doctor of Philosophy
in Electrophysics

June 2009

Hsinchu, Taiwan, Republic of China

中華民國 九十八年六月

III-族氮化物表層缺陷研究

黃國欽¹⁾ 黃凱風²⁾

國立交通大學電子物理所

摘要

在本論文中，我們研究表面缺陷特性以氮化鎵材料為主並藉由蕭特基元件在不同表面處理的條件下探討電流轉換機制及缺陷密度，並利用特徵電阻(Specific contact resistance)、理想因子(Ideality factor)及特性參數(characteristic energy)作分析。另外為了研究表面缺陷對元件的光電性影響，光檢測器的製作與元件特性經由不同表面處理及熱穩定性也將在論文中一一探討。其中元件在沒有經由電漿式耦合蝕刻(ICP)的條件下，電流轉換機制由熱激發式(Thermionic emission; TE)來主導，另一方面，當元件經由電漿式耦合蝕刻(ICP)的處理後，其電流轉換機制將由熱激發式轉而變成場發式(Field emission; FE)來主導，其原因主要是由於元件使用電漿式耦合蝕刻(ICP)後會在元件表面產生表面缺陷而改變其電流轉換機制，而這些由電漿式耦合蝕刻(ICP)產生的表面缺陷可以經由在高溫 600°C 氮氣或 500°C 氫氣下減少並使電流的轉換機制由場發式轉而變成熱激發式，以改善元件的特性。

另外我們使用了電容對頻率(Capacitance-frequency; $C-f$)的方

法去分析元件經由電漿式耦合蝕刻 (ICP) 後所產生的表面缺陷形式，約可分為 s-type、m-type 及 f-type。其中 s-type 的表面缺陷主要是來自於元件經由電漿式耦合蝕刻 (ICP) 處理後所產生的缺陷並可藉由在高溫 600°C 氮氣或 500°C 氬氣下減少，另外 m-type 及 f-type 的表面缺陷是來自於元件本身的磊晶成長缺陷並亦可利用在高溫氮氣或氬氣下降低缺陷密度。

另一方面光檢測器利用電漿式耦合蝕刻 (ICP) 後所產生的表面缺陷及高溫處理後，將可產生較高的光響應及內部增益，其中光檢測器光響應藉由在氮氣高溫合金 400°C、500°C 及 600°C 下各別為 3.95A/W、0.72A/W 及 1.85A/W 與內部增益在氮氣高溫合金 400°C、500°C 及 600°C 下各別為 195、36 及 84。較高的光響應及內部增益主要是由於光檢測器利用電漿式耦合蝕刻 (ICP) 後所產生的表面缺陷及高溫處理後在其元件的材料特性中，有較多的電洞或電子被補捉，當元件操作在高電場及照光下將藉由這些電洞或電子被補捉與增加碰撞機率產生更多的光電子。

- 1) 作者
- 2) 指導教授

Investigation of interfacial defects in III-nitride

Kuo-Chin Huang¹⁾ Kai Feng Huang²⁾

Abstract

The interfacial defects properties of GaN-based Schottky diodes have been investigated and fabricated by utilized current voltage temperature (I - V - T) and capacitance-frequency (C - f) methods. Surface states effects of metal-semiconductor-metal (MSM) photodetectors (PDs) and p-i-n PDs is applied high reverse electrical field in illumination to confirm the relationship between ICP-induced defects and optoelectric devices characteristics in this dissertation. The current transport mechanisms are analyzed in terms of specific contact resistance (ρ_c), characteristic energy (E_{00}) and ideality factor (η) under different annealing temperatures. The current transport mechanisms of non-treated n -type GaN was TE and was FE based on the finding that the sample by using ICP etching processes. However, the current transport mechanisms can be changed from FE to TE by annealing at 600°C in N₂ ambient or 500°C in H₂ ambient, that is, the current transport mechanism dominates TE or between TE and FE. These results showed that the ICP damages were reduced to a low level and the Schottky diodes characteristics recovered by annealing 600°C in N₂ ambient or 500°C in H₂ ambient. In this dissertation, we have found that the current transport mechanisms are directly

dependent on the surface treated conditions, and annealing processes are an effective step in eliminating these defects, and characterize ICP-induced defects such as *s*-type, *m*-type and *f*-type interfacial defects by capacitance-frequency (*C-f*) methods. The *s*-type interfacial defects can be reduced by annealing temperature increasing to 600°C in N₂ ambient or 500°C in H₂ ambient. The *m*-type interfacial defects can be recovered to non-treated *n*-type GaN by annealing at high temperature in N₂ ambient or in H₂ ambient. In *f*-type interfacial defects, annealing in N₂ ambient is more effective than that in H₂ ambient. The interfacial defects of the Schottky diode with ICP induced defect is dominant *s*-type, and non-treated sample is dominant *f*-type. The interfacial defects is *f*-type indicating the ICP induced defects nearly recovered to non-treated sample, this is the defects result from epitaxial growth such as dislocation or the others.

On the other hand, the higher responsivity and internal gain for metal semiconductor metal photodetectors (MSM-PDs) with different surface treatment have been fabricated. The responsivity of MSM-PDs with annealing at 400°C, 500°C and 600°C in N₂ ambient by applying reverse bias -1Volt is 3.95A/W, 0.72A/W and 1.85A/W, respectively. The internal gain of MSM-PDs with annealing at 400°C, 500°C and 600°C in N₂ ambient at a photon energy of 3.35eV by applying reverse bias -1Volt is 195, 36 and 84, respectively. The higher responsivity and internal gain characteristics for MSM-PDs with ICP etching process and annealing in N₂ ambient at different temperatures are clearly observed. This result may attribute to interfacial

states such as holes traps what capture or emit electrons or hole as applied high reverse electrical field and illumination. The persistent photoconductivity effects (PPC) in MSM-PDs with interfacial states by annealing treatment have been studied to confirm the ICP-induced defects exist. Photocurrent gradually increased and the dark current decreased with measured time is observed. These results may also attribute to the presence of holes trap or acceptor-type trap states.


- 1) Author, Department of Electrophysics, National Chiao Tung University
- 2) Advisor, Department of Electrophysics, National Chiao Tung University



誌謝

(Acknowledgements)

學習除了靠自己的努力外，更需要好的環境，在博士求學的階段由衷感謝交通大學給我一個多元化、資源充足的浩然圖書館及修課環境，感謝電子物理所的教授們在學業與物理上的教導，其中更加感謝我的指導老師黃凱風教授及高雄大學藍文厚教授這七年來的鼓勵與指導，在討論的過程中總能帶給我無限的啟發與求知的動力，使我能一路順利的完成學業。另外，感謝陳永富教授及實驗室的學弟妹們、蘇冠緯博士、黃仕璋博士、江建勳、王偉立... 等人的幫忙。



特別感謝中山科學研究院從我碩士到完成博士學歷的這九年期間提供了我一個認識光電半導體領域及學習如何與人相處的環境，讓我從大學畢業對光電、對物理了解不多的新鮮人，到今日可以略知物理的本質與開啟對物理的興趣，其中感謝林文仁博士、程一誠博士、張國仁博士、李大青博士、張善寬、林科均及學長林家慶博士、柯文哲博士、陳文瑞博士、陳一塵博士、柯誌欣博士、官大明博士的鼓勵與協助及多年來在實驗上幫忙的學弟們郭武吉、林季範、黃鍾億、黃皆智、林義峯、藍志學、劉文宏及李漢誠... 等人。

另外特別感謝璨圓光電董事長簡奉任博士及研發處處長潘錫明博士，在修業博士的求學生涯裡提供了一個良好的學習環境與工作上

的包容，讓我可以學以致用在工作上，將工作與學習融為一體，並能從中獲得對物理原理的探討與知識，並感謝這七年來一路陪我走過來的璨圓光電同事們，謝謝你們平時的相處與鼓勵，豐富了我的生命與生活，有你們的日子裡讓我感受到朋友的真諦。

感謝口試委員藍文厚教授、陳振芳教授、陳永富教授、簡奉任董事長、林文仁博士及李晉東博士對本論文的指導與建議。

最後感謝我的父母親及家人們平時對我的包容與關心，從高中時期到今日在外求學總是聚少離多，隨著時間的增長離家越遠回家越少，在此我想告訴我的爸爸媽媽：你們辛苦了，雖然我花了不少時間才完成學業，但我把你們沒有讀的書與夢想完成了。另外在修讀博士期間，特別感謝李卓燕多年來的鼓勵與支持，在課業之餘充實我的精神生活與陶冶心靈，豐富了我的生命與生活，為我的人生寫下值得回憶的樂章。

Contents

Abstract (Chinese)	i
Abstract (English)	iii
Acknowledgments	vi
Contents	viii
Table captions	xi
Figure captions	xii
Chapter 1 Introduction	1
1.1 The research background on GaN	1
1.2 Overview of the our studies	2
Chapter 2 Foundational Theory and physics	7
2.1 Physical and electrical characteristics of metal semiconductor rectifies	
2.1.1 Introduction	7
2.1.2 Theory of current transport mechanisms for Schottky contacts .	8
2.1.2.1 Thermionic emission (TE)	10
2.1.2.2 Field emission (FE)	11
2.1.2.3 Thermionic-field emission (TFE)	11
2.1.3 Current-voltage characteristics of Schottky contacts . .	12
2.1.3.1 Current-voltage (<i>I-V</i>) characteristics by thermionic emission (TE) theory	12

2.1.3.2	Current-voltage ($I-V$) characteristics by thermionic-field emission (TFE) theory	13
2.1.3.3	Current-voltage-temperature ($I-V-T$) characteristics by thermionic emission (TE) theory	15
2.1.3.4	Current-voltage characteristics with series resistance by thermionic emission (TE) theory	16
2.1.4	Capacitance-voltage ($C-V$) characteristics of Schottky contact	17
2.1.5	Capacitance-frequency ($C-f$) characteristics of Schottky contact with interfacial states	19
2.2	Theory and physical characteristics of photodetector	20
2.2.1	Introduction	20
2.2.2	Metal-semiconductor-metal photodetectors (MSM-PDs)	
2.2.2.1	Geometrical structure and physical characteristics	20
2.2.2.2	Responsivity and quantum efficiency	25
2.2.2.3	Shockley-Read-Hall Theory of recombination and internal gain	27
2.2.3	$p-i-n$ junction photodetector	33

Chapter 3	Interfacial states effects and characteristics for Schottky diodes	48
3.1	Introduction	48

3.2 Schottky diodes with annealing nitride and hydrogen effects	49
3.2.1 Current voltage characteristics	49
3.2.2 Current temperature characteristics	53
3.2.3 Capacitance frequency characteristics	58
3.2.4 Summary	63
Chaper 4 Investigation of interfacial states for	
metal-semiconductor-metal photodetectors (MSM-PDs)	
4.1 Introduction	95
4.2 Surface treatment by annealing in N ₂ or H ₂ ambient	96
4.2.1 Internal gain effects for MSM-PDs by surface treatment	96
4.2.2 Persistent photoconductivity effects (PPC) for MSM-PDs with interfacial states	100
4.3 Summary	103
Chapter 5 Application of interfacial states for <i>p-i-n</i>-photodiodes	117
Chapter 6 Conclusions and Future prospects	126
Appendix A References	131
Appendix B Notation	144
Appendix C Detailed experimental discussion	148
C.1 Epitaxial growth for GaN	148
C.1.1 Schottky diodes and metal-semiconductor-metal photodetector	

	(MSM-PDs)	148
C.1.2	<i>p-i-n</i> -photodiodes	148
B.2	Process procedure and conditions	149
C.2.1	Inductively coupled plasma reactive ion etching (ICP-RIE)	
C.2.2	Schottky diodes by ICP-RIE etching processes	151
C.2.3	AlGaN-based <i>p-i-n</i> photodiodes with different surface treatment	155
Appendix D	Current voltage characteristics analysis and simulation by C language tool	158
Appendix E.	Publications	167



Table captions

Table 2-1	Experimental Richardson constant A^* data	40
Table 3-1	Different surface treatment process conditions	66
Table 3-2	Current voltage characteristics of Schottky diodes by annealing at different temperature in N_2 or H_2 ambient	66
Table 3-3	Current temperature characteristics of Schottky diodes by annealing at different temperature in N_2 or H_2 ambient	67
Table 3-4	Summary of the interfacial states characteristics for Schottky contact with/without by annealing in N_2 or H_2 ambient.	67
Table 3-5	Barrier height for sample with different annealing treatment is extracted by different methods.	68
Table 3-6	Dominant type of defects for n -GaN Schottky diodes by different surface treatment	68
Table 4-1	The detailed process conditions for measured PPC effects	112

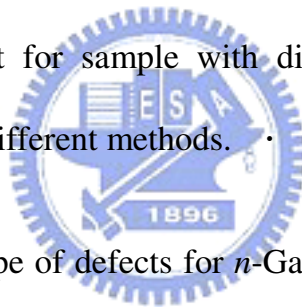
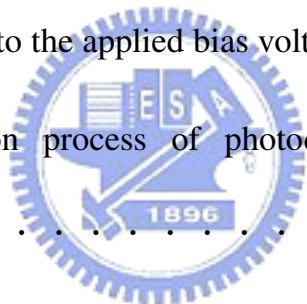


Figure captions

Figure 2-1	Schematic energy band diagram of metal-semiconductor junction 37
Figure. 2-2	Barrier height is depicted as a function of the metal work function and surface treatment. The results of this work are compared to that of other authors. 38
Figure 2-3(a)	Schematic description of the thermionic emission mechanism in <i>n</i> -type semiconductor 39
Figure 2-3(b)	Schematic description of the tunneling mechanisms in <i>n</i> -type semiconductor 39
Figure 2-4	Schematic structure of different type photodetectors . . . 41
Figure 2-5	MSM-PDs with interdigitated electrodes by planar structures 42
Figure 2-6	Equivalent metal-semiconductor-metal photodetectors (MSM-PDs) 43
Figure 2-7	Optical absorption processes in direct band-gap semiconductor. (a) band to band, (b) acceptor level to conduction band, (c) valence band to donor level, (d) acceptor level to donor level, (e) donor level to conduction level and (f) valence band to acceptor level. 43

Figure 2-8	Schematic photoexcitation processes	44
Figure 2-9	Absorption coefficient for $\text{Al}_x\text{Ga}_{1-x}\text{N}$ -based material	44
Figure 2-10	Electrical characteristics for <i>p-i-n</i> photodetectors under reverse bias	45
Figure 2-11	(a) Schematic structure (b) band diagram (c) absorption process of photodetectors under operated reverse bias	46
Figure 2-12	A photoconductive detector with an electrical field is applied to the semiconductor, and the photo-carriers are generated in response to the applied bias voltage.	47
Figure 2-13	Generation process of photodetectors under reverse bias voltage	47
Figure 3-1	Reverse current voltage characteristics of <i>n</i> -GaN Schottky diodes by annealing at different temperatures in N_2 ambient for 30 min	69
Figure 3-2	Reverse breakdown voltage characteristics of Schottky diodes by different surface treatments	69
Figure 3-3	Forward current voltage characteristics of <i>n</i> -GaN Schottky diodes by annealing at different temperatures in N_2 ambient for 30 min	70
Figure 3-4	Current voltage characteristics of <i>n</i> -GaN Schottky diodes	



without ICP etching treatment are fitting and analyzed by Eq. (2-11). 70

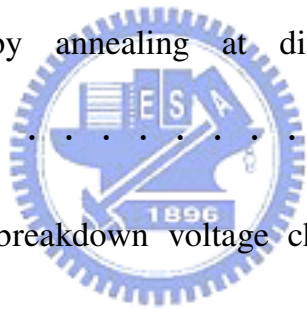
Figure 3-5 Ideality factor and barrier height of Schottky diodes are analyzed by annealing at different temperatures in N₂ ambient. The solid shape donates Schottky diodes without ICP treatment (R1 sample), in contrast the void shape donates Schottky diodes with ICP treatment (R2 sample) by annealing at different temperatures. 71

Figure 3-6 Reverse current-voltage (I-V) characteristics of the Schottky diodes by annealing at different temperatures in H₂ ambient 72

Figure 3-7 Reverse breakdown voltage characteristics of the Schottky diodes by annealing at different temperatures in H₂ ambient 72

Figure 3-8 Forward current voltage characteristics of Schottky diodes by annealing at different temperatures 73

Figure 3-9 Ideality factor and barrier height of Schottky diodes are analyzed by annealing at different temperatures in H₂ ambient. The solid shape donates Schottky diodes without ICP treatment (R1 sample), in contrast the void shape donates



	Schottky diodes with ICP treatment (R2 sample) by annealing at different temperatures.74
Figure 3-10	Current-voltage temperature characteristics of Schottky diodes without ICP treatment (R1 sample) by measuring at different temperatures75
Figure 3-11	Current-voltage temperature characteristics of Schottky diodes with ICP treatment (R2 sample)75
Figure 3-12	Current-voltage temperature characteristics of Schottky diodes with annealing at 400°C in N ₂ ambient (A1 sample)76
Figure 3-13	Current-voltage temperature characteristics of Schottky diodes with annealing at 500°C in N ₂ ambient (A2 sample)76
Figure 3-14	Current-voltage temperature characteristics of Schottky diodes with annealing at 600°C in N ₂ ambient (A3 sample)77
Figure 3-15	Current-voltage temperature characteristics of Schottky diodes with annealing at 700°C in N ₂ ambient (A4 sample)77
Figure 3-16	Ideality factor is extracted by measuring at different temperatures for Schottky diodes with annealing in N ₂ ambient.78
Figure 3-17	Barrier height is extracted by measuring at different temperatures for Schottky diodes with annealing in N ₂ ambient.78



Figure 3-18	Specific contact resistance of Schottky diodes with different surface treatment in N ₂ ambient is indicated as a function of temperature. 79
Figure 3-19	Richardson plot of the Schottky diodes with different surface treatments in N ₂ ambient. 79
Figure 3-20	Current-voltage temperature characteristics of Schottky diodes with annealing at 400°C in H ₂ ambient (B1 sample) . . . 80
Figure 3-21	Current-voltage temperature characteristics of Schottky diodes with annealing at 500°C in H ₂ ambient (B2 sample) . . . 81
Figure 3-22	Current-voltage temperature characteristics of Schottky diodes with annealing at 600°C in H ₂ ambient (B3 sample) . . . 81
Figure 3-23	Current-voltage temperature characteristics of Schottky diodes with annealing at 700°C in H ₂ ambient (B4 sample) . . . 82
Figure 3-24	Ideality factor is extracted by measuring at different temperatures for Schottky diodes with annealing in H ₂ ambient. 82
Figure 3-25	Barrier height is extracted by measuring at different temperatures for Schottky diodes with annealing in H ₂ ambient. 83
Figure 3-26	Specific contact resistance of Schottky diodes with different

surface treatment in H_2 ambient is shown as a function of temperature. 83

Figure 3-27 Richardson plot of the Schottky diodes with different surface treatments in H_2 ambient. 84

Figure 3-28 Frequency dependence of the interfacial states capacitance of the Schottky diodes for non-treated sample (R1) and non-annealed ICP-treated sample (R2). The dot line curve represents the fitting result of the experimental data. . . 84

Figure 3-29 Frequency dependence of the C_p results of the Schottky diodes with annealing at $400^\circ C$ in N_2 ambient after ICP etching process. The dot line curve represents the fitting results. . 85

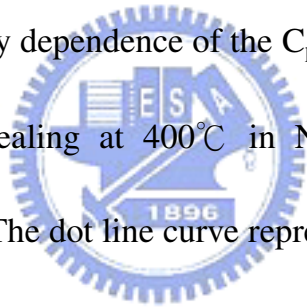


Figure 3-30 Frequency dependence of the C_p results of the Schottky diodes with annealing at $500^\circ C$ in N_2 ambient after ICP etching process. The dot line curve represents the fitting results. . 85

Figure 3-31 Frequency dependence of the C_p results of the Schottky diodes with annealing at $600^\circ C$ in N_2 ambient after ICP etching process. The dot line curve represents the fitting results. . 86

Figure 3-32 Compared with different types of interfacial states by annealing in N_2 ambient, the interfacial states density as a

	function of temperature is observed.	87
Figure 3-33	Frequency dependence of the C_p results of the Schottky diodes with annealing at 400°C in H ₂ ambient after ICP etching process. The dot line curve represents the fitting results.	87
Figure 3-34	Interfacial state capacitance of A1 and B1 sample by annealing at 400°C	88
Figure 3-35	Interfacial state capacitance of B1 and B2 sample by annealing in H ₂ ambient	88
Figure 3-36	Frequency dependence of the C_p results of the Schottky diodes with annealing at 600°C in H ₂ ambient after ICP etching process. The dot line curve represents the fitting results.	89
Figure 3-37	Compared with different types of interfacial states by annealing in H ₂ ambient, the interfacial states density as a function of temperature is observed.	89
Figure 3-38	Capacitance voltage characteristics of Schottky diodes with/without ICP treatment. The dot line represents fitting data.	90
Figure 3-39	Capacitance voltage characteristics of Schottky diodes with annealing in N ₂ ambient at a frequency 1MHz	90

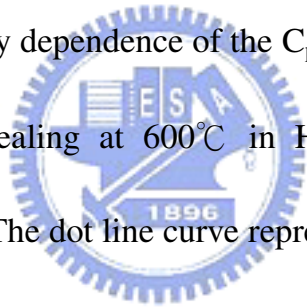
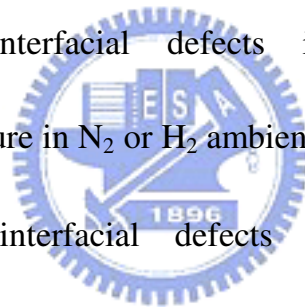
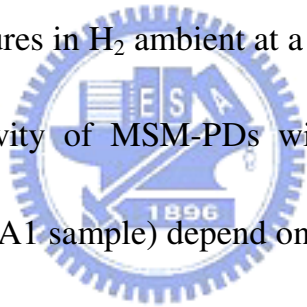


Figure 3-40	Capacitance voltage characteristics of Schottky diodes with annealing in H ₂ ambient at a frequency 1MHz	91
Figure 3-41	Depletion width of Schottky diodes with different surface treatments	91
Figure 3-42	Ideality factor is dependent of annealing temperature for different surface treated samples	92
Figure 3-43	Barrier height is dependent of annealing temperature for different surface treated samples	92
Figure 3-44	<i>s</i> -type interfacial defects is dependent of annealing temperature in N ₂ or H ₂ ambient.	93
Figure 3-45	<i>m</i> -type interfacial defects is dependent of annealing temperature in N ₂ or H ₂ ambient.	93
Figure 3-46	<i>f</i> -type interfacial defects is dependent of annealing temperature in N ₂ or H ₂ ambient.	94
Figure. 4-1	Current voltage characteristics of MSM-PDs without surface treatment	106
Figure 4-2	Current voltage characteristics of MSM-PDs with ICP etching treatment	106
Figure 4-3	Responsivity of MSM-PDs with/without ICP etching	



	treatment	107
Figure 4-4	Responsivity of MSM-PDs with different annealing temperatures in N ₂ ambient	107
Figure 4-5	Internal gain of MSM-PDs with annealing at different temperatures in N ₂ ambient at a wavelength of 370nm . . .	108
Figure 4-6	Responsivity of MSM-PDs with annealing at different temperatures in H ₂ ambient	108
Figure 4-7	Internal gain of MSM-PDs with annealing at different temperatures in H ₂ ambient at a wavelength of 370nm . . .	109
Figure 4-8	Responsivity of MSM-PDs with annealing at 400°C in N ₂ ambient (A1 sample) depend on the finger spacing and reverse bias at wavelength of 370nm.	109
Figure 4-9	Internal gain of MSM-PDs with annealing at 400°C in N ₂ ambient (A1 sample) is depicted as a function of finger spacing at wavelength of 370nm.	110
Figure 4-10	Internal gain of MSM-PDs with annealing at 400°C in N ₂ ambient (A1 sample) is depicted as a function of reverse bias at wavelength of 370nm.	110
Figure 4-11	Internal gain of MSM-PDs with annealing at different	



temperature is depicted as a function of finger spacing at wavelength of 370nm and reverse bias -1.5V. 111

Figure 4-12 Dark current voltage characteristics for MSM-PDs with annealing at 500°C in H₂ ambient (B2 sample). After illuminated a photon energy of 3.35eV, the dark current subsequently was measured without illumination. The detailed measured process flow is described in Table 4-1. . . . 113

Figure 4-13 Photocurrent with applied reverse bias for MSM-PDs with annealing at 500°C in H₂ ambient (B2 sample). After illuminated a photon energy of 3.35eV, the photocurrent subsequently was measured by utilized step by step. . . 113

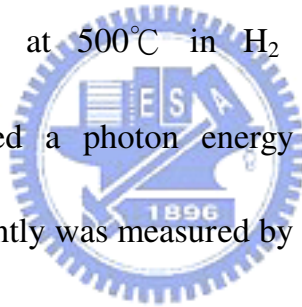


Figure 4-14 Current-time characteristics with a constant reverse bias -2Volt and illuminated a photon energy of 3.35eV. . . . 114

Figure 4-15 Current-time characteristics with a constant reverse bias -2Volt and illuminated a photon energy of 3.26eV. . . . 114

Figure 4-16 Current-time characteristics with a constant reverse bias -2Volt and illuminated a photon energy of 3.1eV. . . . 115

Figure 4-17 Schematic photoexcitation process (a) thermionic emission, (b) field emission, (c) band to band and (d) acceptor level or donor

	level to conduction band in the thermal equilibrium or applied lower reverse bias.	115
Figure 4-18	Schematic photoexcitation process (a) thermionic emission, (b) field emission, (c) band to band and (d) acceptor level or donor level to conduction band in the higher reverse bias.	116
Figure 5-1	Current-voltage (I-V) characteristics of AlGaIn-based photodiode devices (PDs) with annealing at different gases under the illumination ($0.13\mu\text{W}$) is at a wavelength of 330nm. The insert of figure shows a lower dark current could be observed.	121
Figure 5-2	Current-voltage (I-V) characteristics of different annealing treated samples illuminated with a wavelength of 360nm ($0.23\mu\text{W}$).	121
Figure 5-3	Current-voltage (I-V) characteristics of different annealing treated samples illuminated with a wavelength of 400nm ($0.4\mu\text{W}$).	122
Figure 5-4	Spectral response of surface treated samples with different annealing ambient under reverse bias voltage -8 Volt.	122
Figure 5-5	Current-voltage characteristics for as grown and KOH-treated PDs under the illumination ($0.7\mu\text{W}$) with wavelength 330nm	123

Figure 5-6	Current-voltage characteristics for as grown and KOH-treated PDs under the illumination (2.8 μ W) with wavelength 400nm	123
Figure 5-7	Spectral responsivity for as grown and KOH-treated PDs at different biases	124
Figure 5-8(a)	Scanning electron microscopy (SEM) images of the AlGaIn-based photodiodes for the as grown sample after it has been etched to n ⁺ -GaIn region.	125
Figure 5-8(b)	Scanning electron microscopy (SEM) images of the AlGaIn-based photodiodes for the KOH-treated sample after it has been etched to n ⁺ -GaIn region.	125
Figure C.1	OXFORD Plasmalab System 100	151
Figure C.2	Fabrication process flow of Schottky diodes	154
Figure C.3.	The AlGaIn-based photodiode devices structure with different surface treatments.	157